JOURNAL OF GEOPHYSICAL RESEARCH, VOL. 115, A00E29, doi:10.1029/2009JA014761, 2010

Click Here for Full Article

Two-dimensional frequency domain modeling of lightning EMP-induced perturbations to VLF transmitter signals

R. A. Marshall[1,2] and U. S. Inan[3,4]

Received 12 August 2009; revised 11 December 2009; accepted 11 January 2010; published 3 June 2010.

[1] The lightning electromagnetic pulse creates observable modifications to the overlying *D* region ionosphere, exhibited optically as elves. Recent work, both experimental and theoretical, has shown that elves are accompanied by considerable electron density disturbances of up to a factor of 2 increase in local density. We investigate the possibility that these density disturbances are observed by subionospheric VLF transmitter signals as the so-called early VLF events. We use a finite difference frequency domain model to simulate the VLF transmitter signal propagating subionospherically to a VLF receiver, under ambient conditions and through a disturbed region. We show that modeled electron density disturbances, consistent with optical observations of elves, yield small but detectable perturbations to the VLF transmitter signal and may explain at least some observed early VLF events. We further show that sequences of in-cloud lightning pulses, as in spider lightning, may yield considerably higher density disturbances and similarly more prominent VLF transmitter perturbations. In this way, the model herein supports previously reported correlations between sferic bursts and early VLF events.

Citation: Marshall, R. A., and U. S. Inan (2010), Two-dimensional frequency domain modeling of lightning EMP-induced perturbations to VLF transmitter signals, *J. Geophys. Res.*, *115*, A00E29, doi:10.1029/2009JA014761.

1. Introduction

[2] Perturbations to subionospheric VLF transmitter signals known as "early VLF" events have been without a definitive explanation since their discovery by *Armstrong* [1983] and *Inan et al.* [1988]. These perturbations are known to be caused by direct coupling of lightning energy to the ionosphere [*Inan et al.*, 1991] due to their short, <20 ms delay from the causative discharge (hence the name "early"). Since their discovery, attempts to explain the specific cause have included (1) heating and/or ionization due the quasi-electrostatic (QE) field, established by the charge removal in a cloud-to-ground discharge [*Pasko et al.*, 1998]; (2) scattering of the VLF energy from the body of a sprite [*Dowden et al.*, 1996]; (3) "sustained heating" of the ionosphere due to the charge imbalance in the thunderstorm, regularly interrupted by discharges [*Inan et al.*, 1996b]; or (4) combined QE and electromagnetic pulse (EMP) heating and ionization associated with the optical phenomenon known as a halo [*Moore et al.*, 2003]. However, *Marshall et al.* [2006] showed that none of these mechanisms are completely consistent with observations and correlations with optical phenomena. Furthermore, where previously only "early/fast" events were known, having a fast, <20 ms risetime, the discovery of "early/slow" events by *Haldoupis et al.* [2006], with risetimes up to 2–3 s, has created new problems for these mechanisms.

[3] Evidence was shown by *Cheng and Cummer* [2005] and *Cheng et al.* [2007] that the lightning EMP may produce early VLF events. In this work we investigate the possibility that the lightning EMP alone can cause a significant enough ionospheric density disturbance to be measured as an early event in VLF transmitter data. This paper follows on the work of *Marshall et al.* [2008] and complements the work of *Marshall et al.* [2010], wherein a 3-D time domain model was used to calculate the effects of cloud-to-ground and in-cloud lightning on the lower ionosphere, in terms of optical emissions, heating, and ionization. Only ionization changes are consistent with VLF transmitter perturbations: heating alone recovers back to its ambient level in a fraction of a second, while ionization enhancements at *D* region altitudes typically recover in 10–100 s [*Pasko and Inan*, 1994], consistent with observed VLF transmitter perturbations. Hence, in section 4 we use the calculated ionospheric electron density changes from *Marshall et al.* [2010], which are consistent with derived electron density disturbances associated with observed elves [*Mende et al.*, 2005], as an input to our simulations in order to determine their effect on the receiver VLF transmitter amplitude and phase. We investigate the effects of both cloud-to-ground lightning, in-cloud lightning, and sequences of in-cloud pulses, consistent with observed VLF "sferic bursts" [*Johnson and Inan*, 2000; *Marshall et al.*, 2007]. Note that *Cheng et al.* [2007] showed early VLF events for

[1]Center for Space Physics, Boston University, Boston, Massachusetts, USA.
[2]Formerly at STAR Laboratory, Stanford University, Stanford, California, USA.
[3]STAR Laboratory, Stanford University, Stanford, California, USA.
[4]Koç University, Istanbul, Turkey.

Copyright 2010 by the American Geophysical Union.
0148-0227/10/2009JA014761

CG-related EMP only, which are not able to explain early/slow events.

[4] Note that, for the sake of consistency, herein we refer to the modifications to the ionospheric electron density as "disturbances," and changes in the received VLF amplitude and/or phase as "perturbations."

2. FDFD Propagation Model

[5] Most previous work in modeling these perturbations has involved the use of the extensive numerical code known as MODEFNDR [*Pappert and Snyder*, 1972; *Ferguson and Snyder*, 1987], developed by the Naval Ocean Systems Center (NOSC). *Tolstoy* [1983] and *Tolstoy et al.* [1986] used an early 1-D version of MODEFNDR to calculate scattering from regions of enhanced electron density due to lightning-induced electron precipitation (LEP) events. MODEFNDR is one of the components of a package known as the Long Wave Propagation Capability (LWPC), which since the 1980s has been able to account for the effects of mode coupling. In contrast, *Dowden and Adams* [1990, and references therein] used a quasi-2-D, single-mode method to simulate 3-D-described disturbances associated with LEP events. While the LWPC code is inherently 2-D, *Poulsen et al.* [1990] adapted the code to simulate disturbances off the great circle path, albeit for a single mode; this was then adapted to a multiple-mode solution by *Poulsen et al.* [1993]. The full version of LWPC has been used by various authors in this quasi-3-D form to model VLF measurements of ionospheric disturbances [e.g., *Inan et al.*, 1996a, 1996c; *Johnson et al.*, 1999; *Moore et al.*, 2003]. Note that this 3-D method is able to simulate off-path disturbances, but cannot take into account mode coupling within the disturbance.

[6] In this work, we depart from the mode theory of the prior work cited above and apply a recently developed method for modeling perturbations to VLF transmitter signals. All of the prior models used mode theory to solve for the field amplitude at a given receiver location. In this work, a finite difference model is used to directly solve for all six components of the wavefield everywhere in 2-D space. Any discussion of modes and rays is not necessary in this context, since the fields are solved self-consistently, including effects of the frequency-dependent, anisotropic, and inhomogeneous ionosphere and ground. This method provides the advantage of directly solving for fields in both dimensions, and allows us the ability to specify detailed electron density profiles in two dimensions, down to the resolution (i.e., grid cell size) of the simulation space. The downside, of course, is that this 2-D model cannot simulate disturbances off the great circle path, nor can it use information about the lateral size of the disturbance; we will have more to say about those effects later in this paper.

[7] We use the finite difference frequency domain (FDFD) model of subionospheric VLF signal propagation of *Chevalier and Inan* [2006] to simulate VLF signal perturbations. The model consists of a 2-D grid in cylindrical coordinates taking into account the curvature of the Earth. The model uses the magnetized plasma equations described by *Chevalier et al.* [2008, equation (3)], with the static magnetic field, ground conductivity, electron-neutral collision frequency, and electron density defined at all points in the 2-D space. For the static magnetic field a tilted dipole model is used [*Walt*, 1994, pp. 27–31]. The model incorporates variances in the electromagnetic properties of the ground and seawater where relevant along the propagation path. The electron-neutral collision frequency profile can be varied along the path; for the results shown here we use the same profile as *Peter and Inan* [2007], i.e., $\nu(z) = 4.303 \times 10^{11}\, e^{0.1622z}$, where ν is in s^{-1} and z is in kilometers [*Chevalier and Inan*, 2006]. The ambient electron density profile is the same as Profile #2 of *Marshall et al.* [2010], and the disturbed electron density profiles in section 4 are taken from the results of *Marshall et al.* [2010]. Note that this ambient profile is labeled #1 in section 3.4. As described by *Chevalier and Inan* [2006], the propagation path is broken up into segments, with each segment surrounded with a perfectly matched layer (PML) boundary condition to absorb any outgoing waves. The model then makes use of the total field/scattered field method [*Taflove and Hagness*, 2005] to propagate the VLF signal in the forward direction from segment to segment along the path.

[8] VLF magnetic dipole loop antennas oriented toward the source (i.e., with their planes aligned with the great circle path) measure the H_y component; results shown in the remainder of this work thus focus on the H_y component. Note that the model is 2-D only, and so is only able to simulate 2-D disturbances in the ionosphere (i.e., they are infinite in the third dimension), and cannot model scattering in the azimuthal direction, or the effects of off-path disturbances.

3. Simulation of Ionospheric Disturbances

[9] Figure 1 illustrates the method for estimating VLF transmitter signal perturbations using the FDFD model described above. First, "ambient" field patterns are computed over the simulation space of interest through a first run of the model; in the case of Figure 1, this is a path from the NAA transmitter in Maine to a VLF receiver in Parker, Colorado, about 3000 km away, including the realistic ground conductivity parameters along that path. The input ambient electron density is that shown in the inset of Figure 1 (first panel), repeated along the path. The output ambient H_y field is shown in the second panel, and the third panel shows the H_y field amplitude sampled along the ground. This is the amplitude that would be measured by a VLF receiver at any distance from the transmitter; for instance, a receiver at 1000 km along the path, measured from the transmitter, would measure H_y to be about −100 dB relative to 1 μT, or 10 pT, while a receiver at the end of the path, at 3300 km, would measure −105 dB, or about 6 pT.

[10] The first panel shows the fully specified 2-D electron density used in the model, along with a 1-D profile. For the ambient case, the disturbance (labeled as Ionization and Attachment) is not present. To simulate a perturbation, a disturbance is input into the electron density in the first panel as shown. Note, however, that the particular disturbance shown is not a simulation output, but rather is used for illustrative purposes only. This artificial disturbance is Gaussian with a radius of 80 km (where the disturbance is 10% of its maximum). This electron density change is manifested through changes to the 2-D conductivity profile, through the modified electron plasma frequency $\omega_{p,e}$. However,

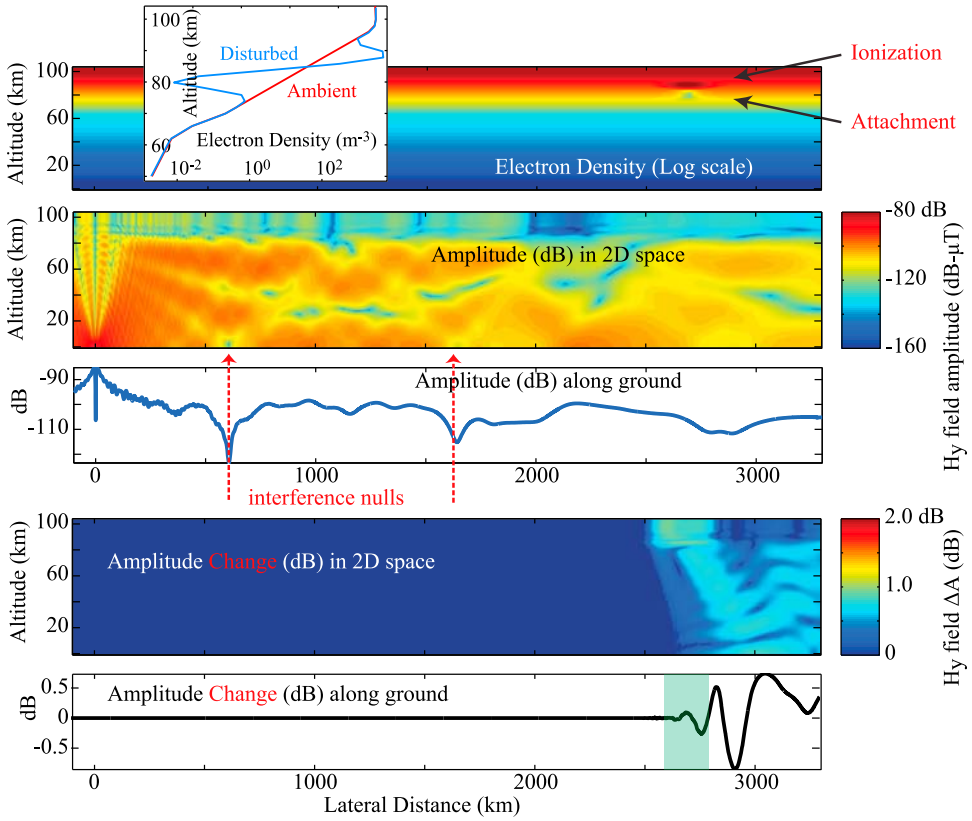


Figure 1. Typical perturbation results from the propagation model. The first panel shows the 2-D electron density, with a disturbance imposed 600 km from the end of the path; the ambient and perturbed 1-D electron density profiles are shown in the inset. The second and third panels show the ambient H_y fields in 2-D space and along the ground, respectively; the fourth and fifth panels show the perturbed fields in two dimensions and along the ground. The green swath centered at 2700 km in the fifth panel shows the lateral location of the disturbance. Note that the same ambient electron density profile has been used for all simulations in this paper.

the collision frequency profile is left unchanged; as such the contribution of the modified electron density to the collision frequency is not considered. The model is then rerun, and outputs similar to the second and third panels are computed. The fourth and fifth panels in Figure 1 show the difference between the ambient and "perturbed" 2-D and 1-D (along-ground) signals. These are by definition the "scattered" fields due to the disturbance. The green swath in the fifth panel simply demarcates the disturbance location (although the disturbance is 85 km above). Note that regions of misleadingly high perturbed amplitude (dB) may appear when the unperturbed field amplitude is low (i.e., near nulls); this problem is discussed in greater detail later in this paper.

[11] A receiver located at any distance from the transmitter measures an early VLF perturbation event with amplitude given in the fifth panel. For example, a receiver at 2000 km measures no perturbation, while a receiver located at 3000 km measures as high as a 0.7 dB perturbation.

[12] A comment must be made about the possible use of this model to simulate backscatter, as observed in data of *Dowden et al.* [1994] and *Marshall et al.* [2006]. In its present configuration, the segmented long path (SLP) model prevents us from accurately measuring backscatter from disturbances. The SLP configuration uses the rightmost fields of one segment as the input to the next segment, but the scattered fields that return to the input (left) side of the segment are not used further. As such, the model calculates scattering in all directions in the 2-D plane of the page in a single segment, but the backscattered fields are not pursued back into the previous segment. The exclusion of backscatter is not likely to be a problem for these events, however. The disturbances used are all "smooth," with slowly varying electron density on scales of tens of km (on the order of a VLF wavelength), and so forward scattering is expected. Furthermore, if significant backscatter were excited, one could expect to see a discontinuity in the field pattern (i.e., the fourth panel of Figure 1) where the backscattered fields stop without reentering the previous segment. Such discontinuities are not observed in our results, either in Figure 1 or any of the examples shown in this work. For this reason we conclude that backscatter is not excited by these disturbances.

3.1. Finite Width Disturbances

[13] Using the LWPC code modified into a 3-D form, *Poulsen et al.* [1990] investigated the effects of varying lateral width disturbances (i.e., the radius of disturbance perpendicular to the great circle path). Those authors found that the perturbation ΔA increased significantly as the radius of the disturbance increased, by a factor of 6 as the radius increased from 2.5 to 7.5 wavelengths; at 20 kHz, that

corresponds to disturbances of 37.5 to 112.5 km lateral width. This result is expected since scatterers on the order of a wavelength scatter isotropically, thus scattering less energy toward the receiver, while scatterers much larger than a wavelength primarily forward scatter [*Johnson et al.*, 1999].

[14] The current model cannot simulate finite-width disturbances; rather, the disturbance is assumed to be infinite in lateral dimension. However, the experimental disturbances considered (produced by *Marshall et al.* [2010]) are typically 150 km or more in lateral dimensions (i.e., 10 wavelengths), and so forward scattering is expected; thus, while a finite-width disturbance might be expected to reduce the scattered amplitude at the receiver, we expect the reduction to be small. Note, however, that *Lev-Tov et al.* [1996] found a reduction in perturbation amplitude by about a factor of 2 when the disturbance is reduced from 300 km to 150 km.

[15] The development of a 3-D version of this model would enable us to simulate off-path disturbances and finite-width disturbances; however, it is likely to be computationally expensive. The current 2-D model runs a 5000 km path in ~12 CPU hours; for a third dimension of ~100 cells, this would require a 100-fold increase in CPU time.

3.2. Effects of Disturbance Location

[16] It was postulated by *Haldoupis et al.* [2004] and *Marshall et al.* [2006] that the location of the electron density disturbance along the transmitter-receiver path would affect the presence or lack of an "event" at the receiver. Most of the events analyzed by *Marshall et al.* [2006] came from the Holographic Array for Ionospheric Lightning (HAIL) [*Johnson et al.*, 1999] and the NAA transmitter in Cutler, Maine; the path from NAA to HAIL is around 3000 km, and most events were no more than 800 km from the receiver array (as they were studied in the context of sprite observations). These events could thus be labeled "near-receiver" events. On the other hand, *Haldoupis et al.* [2004] analyzed events in Europe that were typically within ~500 km of the HWU, HWV and DHO transmitters on which they were observed, while the primary VLF receiver at Crete was some ~1500 km away. These events could in turn be labeled "near-transmitter" events. This difference in experimental setup could then account for the difference in correlation between these two data sets: whereas *Haldoupis et al.* [2004, 2006] found a "one-to-one" correlation between sprites and early VLF events, *Marshall et al.* [2006] found that closer to ~60% were correlated. The difference between these experimental results will be discussed in more detail in section 4.2; here we investigate the effect of the location of the disturbance along the transmitter path.

[17] The fifth through seventh panels of Figure 2 show the change in amplitude along the ground due to disturbances in the ionosphere centered 500, 1000, 1600, 2000, and 2600 km from the receiver. In each of these panels, the green swath marks the lateral location of the disturbance, as in Figure 1. The disturbance itself (i.e., the electron density change) is the same as used in Figure 1. In each case, the disturbance in the ionosphere is identical. The first and second panels simply repeat the ambient 2-D and 1-D along-ground amplitudes in order to see the alignment of interference nulls. The results shown are for the NAA transmitter signal to a VLF receiver at Parker, Colorado. The table at right shows the amplitude change at the receiver and the maximum amplitude achievable, measured at the red dashed lines.

[18] This example demonstrates that the disturbance and receiver locations play a controlling role in determining the received VLF amplitude perturbation, as was also shown by *Lev-Tov et al.* [1996]. The 1000 km case shows almost zero received ΔA and a small maximum ΔA, because the disturbance falls in the middle of a strong-signal region. The 1600 km case, on the other hand, falls near an interference null, yielding a very high maximum ΔA. In the cases where the disturbance is farther from the receiver, the maximum ΔA occurs at the interference null as the scattered signal passes over it. Note that for most of the data presented by *Marshall et al.* [2006], the disturbances fall in the 500–1000 km range from the receiver, on a path of about 3000 km in length. Note also that interference between the scattered modes makes the received amplitude change difficult to predict, as it varies from positive to negative (and passes through zero) at multiple locations along the path. The case in the last panel of Figure 2 corresponds the closest to the cases studied by *Haldoupis et al.* [2004], i.e., near-transmitter disturbances. In the interest of brevity, however, we will not pursue a detailed study of those type of events in this paper, instead leaving it for future work.

[19] Note that the scattered fields themselves depend on the incident field amplitude that reaches the scatterer. Hence, when the disturbance falls into regions where the incident field is low due to interference nulls at ionospheric altitudes (i.e., in Figure 2, the dark region from ~2000 to 2200 km), the scattered field will be smaller. This effect may contribute to the small perturbation amplitude in the 1000 km case, and may also affect the results in the subsequent simulations. In measured data, the presence of these high-altitude "nulls" may suppress early VLF events in some cases, even when a significant disturbance is created.

3.3. Effects of Transmitter Frequency

[20] Equations (11.55), the E field amplitude in the waveguide, and (8.4), the fundamental equation of mode theory of *Budden* [1961] suggest that the interference patterns of the electric and magnetic fields are affected significantly by the transmitter frequency. Furthermore, *Ratcliffe* [1959, Figure 12.1] shows that different frequencies reflect at slightly different altitudes, and so lower-frequency transmitters may probe the higher-altitude regions of the electron density disturbances in the work by *Marshall et al.* [2010] with greater efficiency. However, this effect is likely to be small, as the reflection height changes only very slightly over the frequency range of VLF transmitters. If the VLF reflection height is taken as the altitude at which $\omega_p^2/\omega^2 = \nu/\omega$ [*Ratcliffe*, 1959, Figure 12.1], then for the profiles used in this work, that altitude varies from 84.0 km at 15 kHz, to 84.4 km at 20 kHz, and as high as 85.7 km at 40 kHz.

[21] Figure 3 shows the 2-D and 1-D along-ground H_y field amplitudes for transmitter frequencies from 18 kHz to 30 kHz, in 2 kHz increments, again using the disturbance shown in Figure 1. The VLF transmitters commonly used range from 18.3 to 25.2 kHz, with a few exceptions from 35.0 to 46.0 kHz. While the actual transmitters each have their own distinct location around the globe, each of the

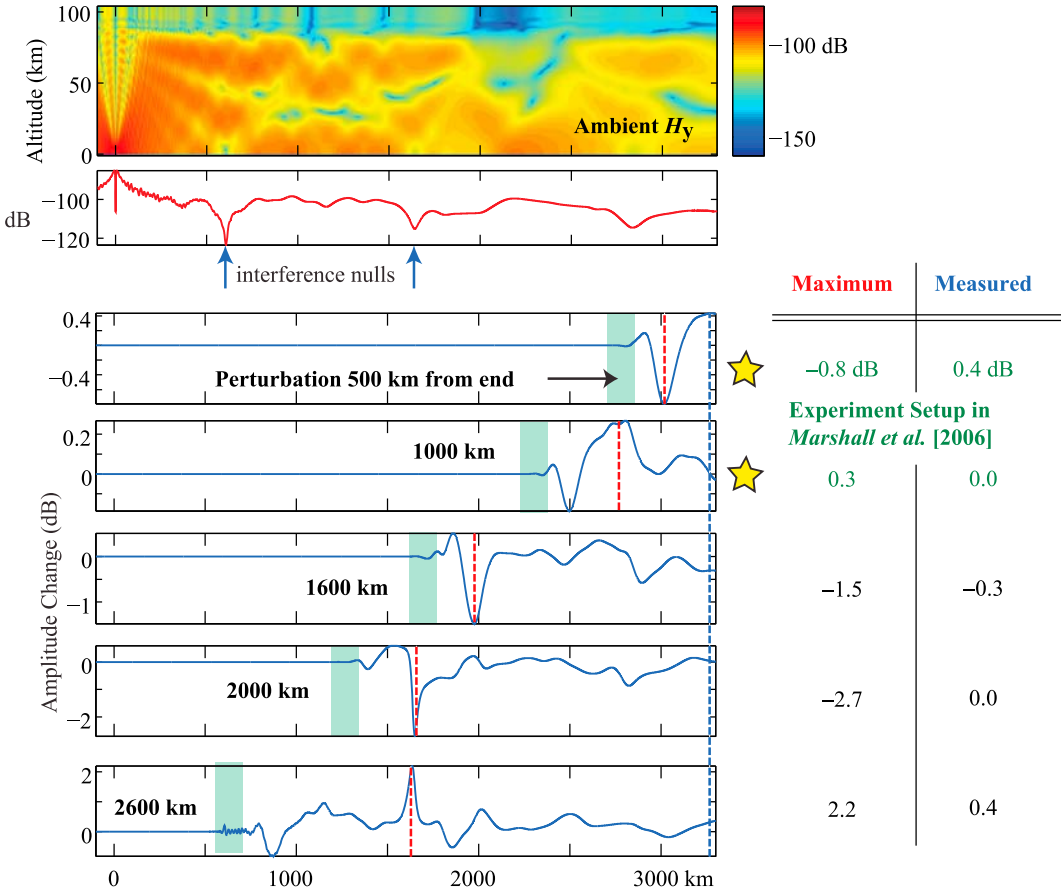


Figure 2. Effect of disturbance location on received amplitude. The first and second panels show the ambient H_y field in two dimensions and along the ground. In the third through seventh panels, five simulations are shown with disturbances at different distances measured from the receiver (right end, blue dashed line). The red dashed line in each plot shows where the maximum perturbation occurs; these values are tabulated at the right. The first two cases (starred), with perturbations at 500 and 1000 km from the receiver, correspond to the experiments by *Marshall et al.* [2006].

simulations in Figure 3 uses the path from the NAA transmitter location in Maine to a receiver in the direction toward Colorado (and beyond), in order to isolate the effect of the transmitter frequency.

[22] Figure 3 shows that the qualitative properties of the transmitter signal vary in a regular way as the frequency is increased. The interference nulls, both along the ground and in the 2-D pattern, tend to move farther from the transmitter as the frequency is increased, as demarcated by the red dashed lines. Furthermore, some nulls disappear altogether, while others appear at higher frequencies only. Ultimately this behavior shows that the frequency of the probe VLF signal has a strong influence on the ambient signal amplitude at a given receiver, in part due to the locations of interference nulls.

[23] Figure 4 shows the results of perturbation simulations using the same frequencies shown in Figure 3. Each of these uses the electron density disturbance from the E_{100} = 40 V m^{-1} vertical discharge case from *Marshall et al.* [2010]. Note that E_{100} is the electric field measured on the ground 100 km from a cloud-to-ground discharge, and according to *Orville* [1991] it is proportional to peak current, in the transmission line model of the lightning return stroke: E_{100} = 0.3 I_k, where I_k is the peak current in kA.

[24] Results show that the perturbations depend strongly on the transmitter frequency, as exhibited in a number of ways. First and most obvious is the presence or lack of interference nulls. In Figure 3, A–D point out prominent interference nulls near the receiver end of three of these paths. In Figure 4, at the locations of the nulls A–D we see prominent spikes in the scattered amplitude, exactly as seen in Figure 2. In the 18 kHz case, the locations marked A and B jump to over 1 and 2 dB, respectively. In the 26 and 28 kHz cases, the amplitudes reach over 5 dB. This large value is consistent with the depth of the interference nulls seen in Figure 3. Figure 4 zooms in on these perturbations for the following discussion.

[25] Apart from the interference nulls, the received amplitude change ΔA is also affected more simply by the transmitter frequency because of the different mode interference in the transmitter signal. Hence, while the 20 kHz case shows a maximum perturbation of only 0.08 dB, the 30 kHz can reach 0.6 dB. While Figure 4 deceptively appears to yield a trend of higher frequency yielding stronger perturbations, other simulations not shown here, with different

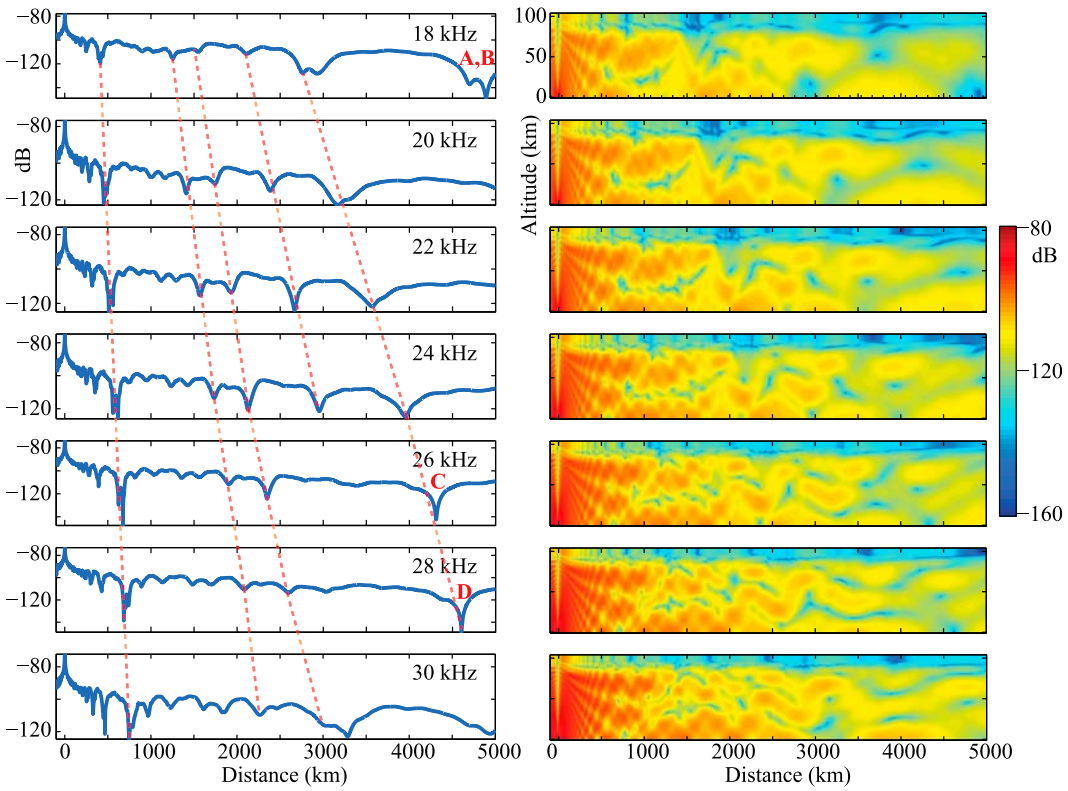


Figure 3. VLF signal amplitudes in two dimensions and one dimension along ground for a variety of transmitter frequencies, corresponding to the typical range of 18–30 kHz used for most VLF transmitters. The red dashed lines show how the location of nulls varies with frequency; A–D correspond to null locations to be discussed with Figure 4.

paths and different electron density disturbances, show this trend to not be the universal case. In fact, there seems to be no frequency that is any "better" than any other at producing measurable perturbations.

3.4. Effects of Ambient Ionospheric Profile

[26] In each of the simulations described so far in this paper, the same ambient ionospheric profile (as shown in the inset in Figure 1 (first panel)) has been used. This profile is a commonly used ambient nighttime ionospheric profile, as calculated using the International Reference Ionosphere (IRI) model for a midlatitude, springtime ionosphere at midnight; it is the same as Profile #2 from *Marshall et al.* [2010], although it is labeled #1 here. However, the background ionospheric profile significantly affects both the lightning EMP–ionosphere interaction as well as the VLF transmitter propagation effects.

[27] The effect of the ambient ionosphere on the lightning EMP–ionosphere interaction was investigated by *Marshall et al.* [2010], as well as in previous work [*Taranenko et al.*, 1993; *Barrington-Leigh et al.*, 2001]. *Marshall et al.* [2010] compared simulations for three different ionospheric profiles and found that the more tenuous profiles resulted in more significant disturbances (as a percentage of the background) compared to dense profiles. This is in wide agreement with previous results and theory; a more dense profile shields the ionosphere, reflecting more of the incident EMP energy, while its higher density simply results in lower-percentage modification, even if the total number of excitations of atmospheric constituents (i.e., ionization or attachment events) is the same.

[28] Previous works in modeling VLF propagation in the Earth-ionosphere waveguide have investigated the effects of different ionospheric profiles. Most recently, *Moore et al.* [2003] used three ionospheric profiles and found that the most tenuous profiles tended to yield the largest amplitude perturbations, while the dense profile yielded very small perturbations. However, this trend was far from predictable; in some cases a more dense profile yields a larger perturbation. The lack of regularity in such simulations can again be attributed to interference between modes: as the ionospheric profile is modified, so is the mode structure in the waveguide.

[29] Figure 5 shows results for simulations with five different electron density profiles. Profile #1 corresponds to the typical nighttime profile used in all other simulations in this paper. Profile #2 is slightly overdense, while Profile #3 is very overdense, such as might occur after a large lightning-induced electron precipitation (LEP) event; these three profiles (#1–3) are the same as those used by *Lev-Tov et al.* [1995]. Profile #4 is slightly underdense, and Profile #5 is very underdense. The top right panel shows the amplitude along the ground for the same 5000 km path as used earlier, for the ambient case (i.e., no disturbance present); one can see that the electron density profile significantly affects the

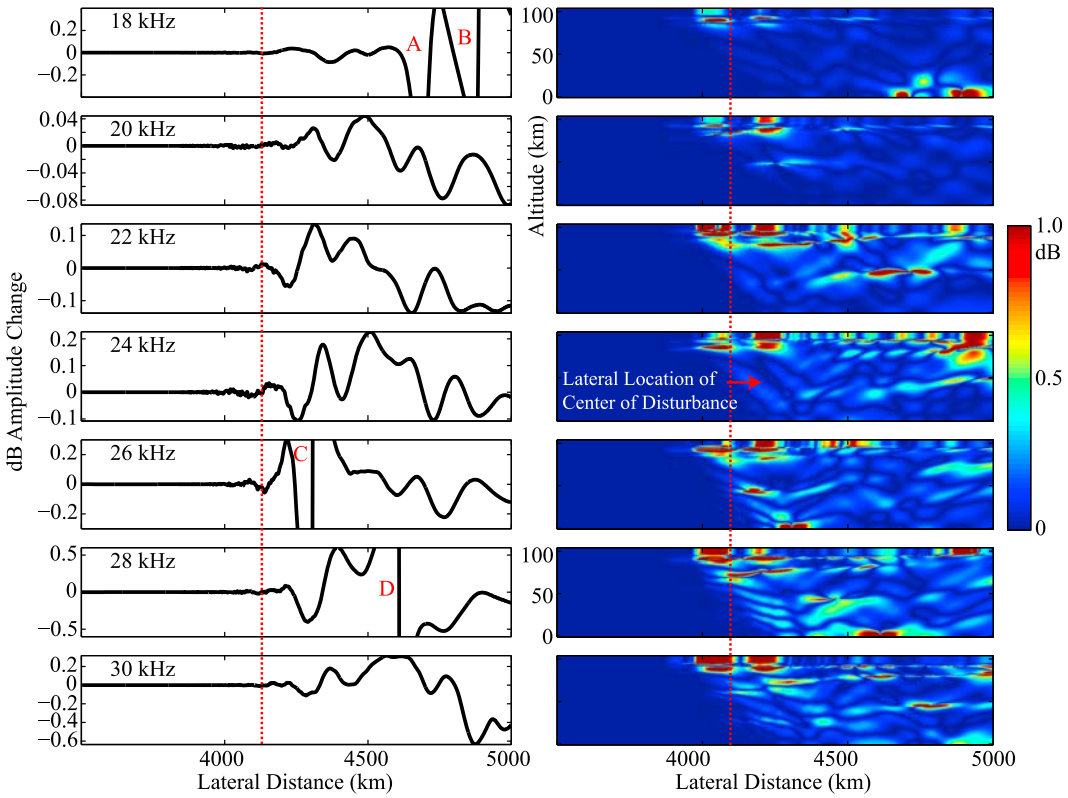


Figure 4. Effect of transmitter frequency on received amplitude. (left) The 1-D amplitude along the ground for simulations from 18 kHz to 30 kHz in 2 kHz increments and (right) the 2-D scattering patterns. A–D correspond to the locations of prominent interference nulls in the ambient field pattern. Note that the panels have been cropped; near these interference nulls the perturbation amplitude can reach 5 dB or higher in some cases.

amplitude received at any point along the ground, and shifts the nulls' locations.

[30] The bottom panels in Figure 5 show the results after including the electron density disturbance from Figure 1. This disturbance was adjusted so that it applied the same *percent change* to each ambient electron density profile. These are likely unrealistic disturbances for some of these profiles: we have forced them to the same percentage to allow comparison. These results show that, apart from the very overdense Profile #3, the electron density profile does not significantly alter the results. Profiles 1, 4, and 5 all yield similar patterns, especially in the 1-D along-ground view, with similar amplitudes in the range −0.5–1 dB. Profile #2 is somewhat similar also, though reaches as high as 2 dB below the disturbance, on account of the prominent null at that location. Profile #3 is unique in its amplitude along the ground (top right panel); it does not appear to exhibit a null pattern like the other profiles. The scattered amplitude along the ground peaks at 5000 km due to a prominent null, but otherwise the perturbation measured is only ~0.2 dB along the ground. Nonetheless, the results here suggest that for typical fluctuations of the nighttime electron density, for a given disturbance, the detectability and absolute amplitude of early VLF events will not be significantly affected. It must be noted, however, that the disturbance itself depends very strongly on the ambient ionospheric profile, as shown by *Marshall et al.* [2010]; the resulting measured perturbation may be reduced, as shown by *Moore et al.* [2003], but the effect comes from the disturbance itself, not from the VLF scattering problem.

4. Results From Simulated Disturbances

[31] In the remainder of this paper, we show simulations of the subionospheric VLF propagation using disturbances calculated by *Marshall et al.* [2010].

4.1. Perturbations From a Single CG Discharge

[32] In the work by *Marshall et al.* [2010], the effects of a single CG discharge interacting with the ionosphere were presented, yielding the typical "elve" optical emissions and associated electron density changes. *Mika et al.* [2006] showed that only a subset of elves had associated early VLF events. From the data presented therein, it is not clear whether the density disturbances underlying elves are due to the EMP (and are thus associated with the elve) or due to associated quasi-electrostatic heating or a burst of in-cloud lightning pulses (and hence could instead be associated with a sprite or sferic burst). In fact, a number of the cases studied by *Mika et al.* [2006] had onset times of up to 2 s, suggesting in-cloud sources. Here, we investigate whether or not the electron density disturbance caused by a single CG discharge could be observed as an early VLF event.

[33] Figure 6 shows simulation results using the single-discharge, vertical EMP results of *Marshall et al.* [2010, Figure 7], and extending to higher amplitudes of E_{100} = 35

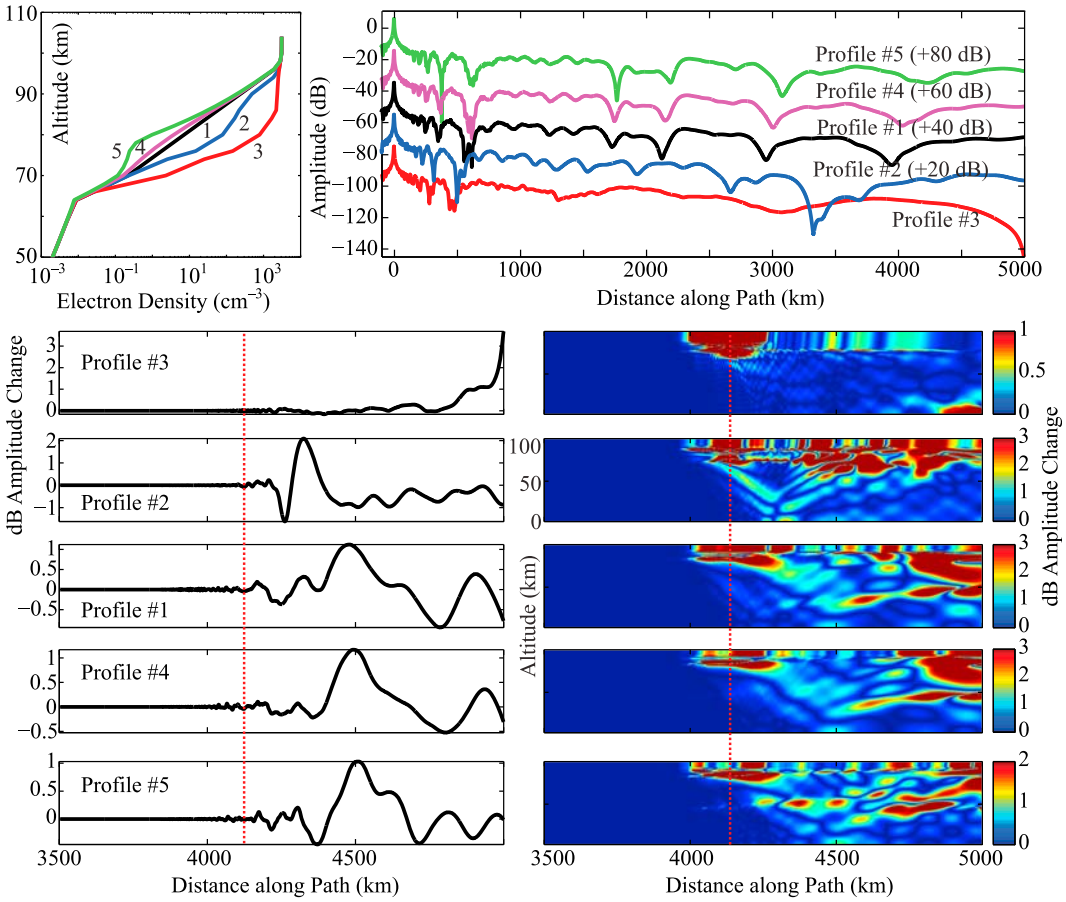


Figure 5. Effect of ionospheric electron density profile on received amplitude. The top left panel shows the 1-D electron density profiles used; the top right panel shows the amplitude along the ground for a 5000 km path. Note that Profiles 1, 2, 4, and 5 have been shifted up. The bottom left panels show the 1-D amplitude along the ground for each profile; the bottom right panels show the 2-D scattering patterns. All other simulations in the paper use Profile #1.

and 40 V m^{-1}. The density disturbance created by these discharges has a roughly toroidal shape with an outer diameter of ~250 km and an inner diameter of ~100 km, and is confined to the altitude range of ~85–92 km. The density enhancement due to ionization has a maximum of 1.0%, 4.0%, 10%, 22%, and 43% for 20, 25, 30, 35, and 40 V m^{-1} pulses, respectively. These disturbances were produced by a pulse of the form $I(t) = I_0 \cosh^{-1}[(t - t_0)/\tau]$ with the half-width τ = 10 μs, impinging on the same ambient ionospheric density profile shown in Figure 1.

[34] The top two panels of Figure 6 show the ambient 2-D and 1-D along-ground H_y field amplitude for reference; these panels are repeated in Figures 7 and 8. The bottom panels show the 2-D scattered H_y field in dB (right) and the 1-D along-ground scattered field, ΔA, also in dB (left). In these examples, the propagation path has been extended to 5000 km in order to avoid interference nulls, which may produce misleadingly high amplitude changes. The path is extended simply to find a region of the simulation space where there are no prominent nulls between the disturbance and the receiver; hence, the region from ~3000 to ~3700 km would also be appropriate, but would limit the available choice of disturbance locations to ~700 km from the receiver. This phenomena of interference nulls and their effect on perturbations is explored in section 3.2 in more detail. Here the disturbance is located 900 km from the receiver end of the path, past the last interference null.

[35] Note that the scattered field patterns for these five simulations show very similar qualitative features, with the amplitude increasing by about a factor of 2 for each 5 V m^{-1} increase in the input field amplitude. We note that the electron density changes in the work by *Marshall et al.* [2010] also increased by about a factor of 2 at each step, so the VLF transmitter signal perturbation here appears to increase approximately linearly with electron density change. Furthermore, upon inspection of the 1-D scattered fields at left, the pattern seems to evolve in a regular way from the E_{100} = 20 V m^{-1} case to the 40 V m^{-1} case; certain fluctuations increase and decrease from one panel to the next.

[36] *Mika* [2007, p. 129] presents a VLF signal perturbation of 0.2–0.4 dB (the exact amplitude change is somewhat difficult to measure) associated with an elve, caused by a +CG of 119 kA (corresponding to $E_{100} \simeq$ 36 V m^{-1}). The results in Figure 6 agree very well with these measurements; a maximum ΔA of 0.2 dB is achieved at multiple locations along the path. This agreement helps explain why only a few elves are associated with VLF perturbations [*Mika*, 2007],

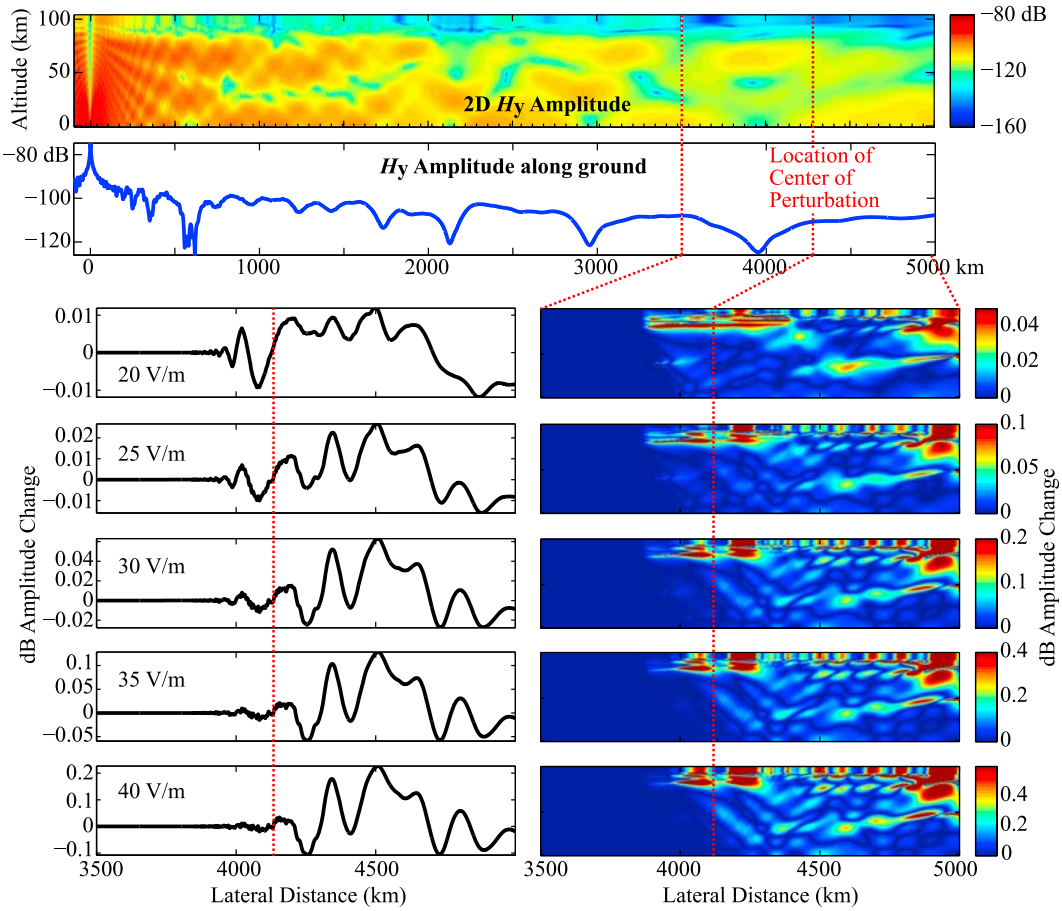


Figure 6. VLF transmitter propagation simulation with CG inputs. The top two panels repeat the ambient 2-D and 1-D along-ground amplitudes. The bottom panels show the scattered 2-D and 1-D fields for the EMP cases of *Marshall et al.* [2010] as well as two more at E_{100} = 35 and 40 V m^{-1}.

since at many locations the amplitude changes would be smaller than detectable levels. The results here demonstrate that only the largest CG strokes can produce measurable disturbances, and thus that only the brightest elves should have associated perturbations; for lightning CGs with E_{100} intensity below 35 V m^{-1}, the perturbation amplitude is below the measurement threshold. However, in cases where the disturbance is near interference nulls, the amplitude change may reach measurable levels, as investigated in section 4.2.

[37] The EMP-induced density changes calculated by *Marshall et al.* [2010] and used here are possibly on the lower side, due to the choice of pulse duration; the pulses used therein have a ~20 μs duration, while a typical +CG return stroke has closer to a 100 μs duration [*Berger et al.*, 1975]. For longer pulses, higher-density changes will likely occur as the ionization enhancement accumulates in time; the resulting perturbations to the VLF transmitter signal may be correspondingly greater. However, this affect may be offset by a reduction in the perturbation amplitude due to the finite lateral width of the disturbance, as described in section 3.1. The quantitative assessment of both of these effects is the subject of ongoing research.

4.2. Perturbations From Sequences of IC Discharges

[38] The hypothesis was put forth by *Marshall et al.* [2008] that many early VLF perturbations could be the signature of electron density changes induced by a sequence of many in-cloud lightning discharges. In this section, that hypothesis is tested.

[39] The 3-D perturbations calculated by *Marshall et al.* [2010], and shown in their Figure 13, are imposed on the 2-D electron density here as described in section 3 by taking a slice through the center of the disturbance. Figure 7 shows results for the 5000 km long simulation space with a transmitter frequency of 24 kHz, where interference nulls have been avoided as described above; the electron density disturbance has again been placed 900 km from the receiver end of the simulation space. The first three cases correspond to sequences of 60 pulses at 5 km altitude, with amplitudes of E^{ic}_{100} = 5, 7 and 10 V m^{-1}, as defined by *Marshall et al.* [2010]. In each of these cases, the disturbance is approximately circular with a diameter of ~100–150 km, altitude extent of ~85–92 km, and maximum density changes of −7%, 50%, and 400% for the three cases, respectively. The fourth case shown here corresponds to a sequence of 100 "random" pulses, with statistics for amplitude, altitude, and orientation given by *Marshall et al.* [2010, Figure 14]; this

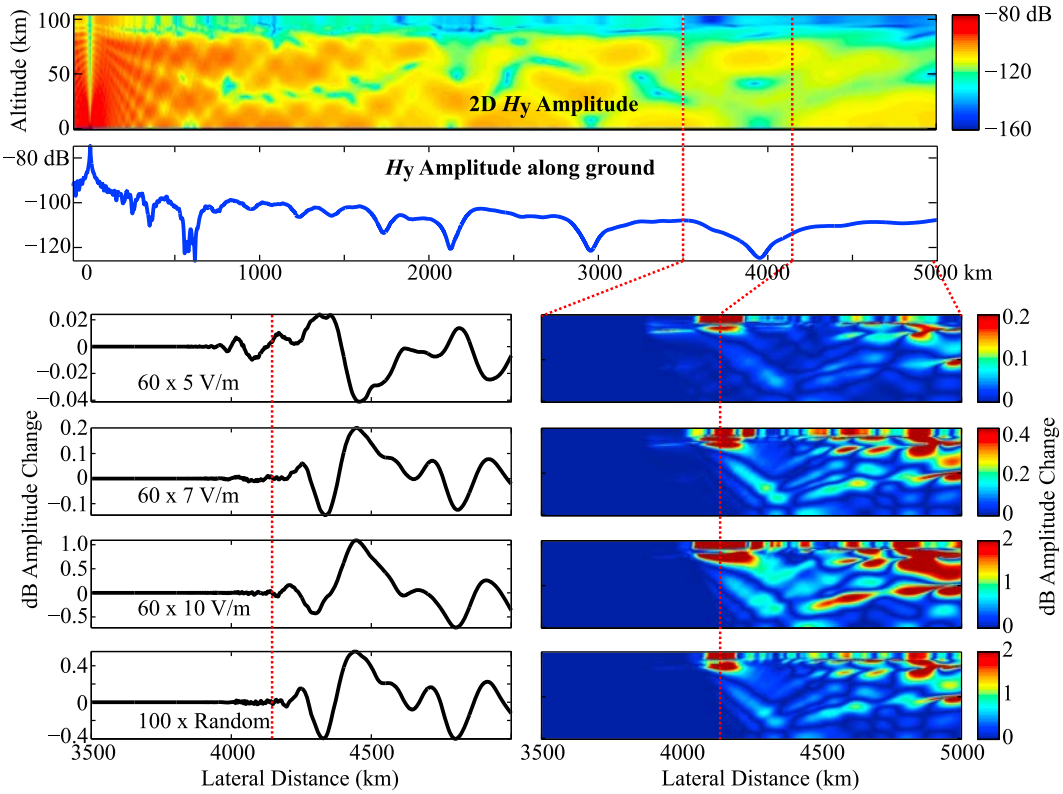


Figure 7. VLF transmitter propagation simulation with EMP multipulse inputs. The top two panels repeat the ambient 2-D and 1-D along-ground amplitudes. The bottom panels show the scattered 2-D and 1-D fields for the four cases of *Marshall et al.* [2010]. The location of the center of the disturbance is denoted by the vertical dashed red line in the bottom panels.

last case attempts to simulate a "realistic" in-cloud lightning event. The parameters for this event are taken from data, described in detail by *Marshall et al.* [2010]. This disturbance has the same physical dimensions as the other three cases, and a maximum density change of 200%. All of the pulses used to create these disturbances had the same temporal width of ~26 μs, using the pulse shape described in section 4.1.

[40] While the 1-D and 2-D patterns have greater variation than in Figure 6, there once again seems to be considerable consistency in the mode interference pattern, especially for the E_{100}^{ic} = 7 V m^{-1}, 10 V m^{-1}, and random cases. Once again, we see that the amplitude change ΔA becomes both positive and negative, and is zero in places. However, except for the E_{100}^{ic} = 5 V m^{-1} case, the absolute amplitude changes are in the measurable range, with the 7 V m^{-1} case reaching 0.2 dB in places. Note, once again, that this 5000 km long path is designed to avoid the misleadingly high ΔA measurements due to nulls (by using a region of the simulation space where there are no interference nulls between the perturbation and the receiver), and so amplitude changes shown here will be at the lower end of observed values in cases where the receiver falls near an interference null.

[41] To illustrate the effects of having the receiver near a null, Figure 8 places the same electron density change 500 km from the receiver end of a 3000 km path; this configuration corresponds to that from the NAA transmitter in Maine to Parker, CO. The ambient 2-D and 1-D fields are identical to the first 3000 km of the previous simulation in Figure 7. Note that an interference null is present very close to the receiver; as such we might expect large ΔA values at the receiver. However, *Johnson et al.* [1999] state that their measurements and simulations do not exhibit a deep null near the receivers. This discrepancy is likely very sensitive to the ionospheric profile used in these simulations.

[42] The simulation results indeed show the expected large amplitude changes. Right at the interference null, where the signal amplitude is low, the relative change in amplitude in dB is very high, reaching 0.2 dB even for the 5 V m^{-1} case, and 1 dB and higher for the 7 V m^{-1}, 10 V m^{-1}, and the random cases. Exactly at the receiver the ΔA drops considerably as the signal amplitude is larger, but the measured values are still 0.3 dB, 2 dB, and 1 dB for the 7 V m^{-1}, 10 V m^{-1}, and the random cases, respectively. The conclusion we draw from this result is that some large measured perturbations may be due to relatively small electron density changes, but enhanced ΔA due to proximity to an interference null. However, it is important to note that the location of this null is sensitive to the ground and ionosphere parameters, as well as the transmitter frequency, as shown in Figure 3, and thus the actual location may be difficult to predict for any particular event. Furthermore, it should be noted that some of the published work using the HAIL array [e.g., *Johnson et al.*, 1999; *Moore et al.*, 2003] claim that no interference null was present near the receiver. However, many published cases exist for which the presence or lack of nulls in not known.

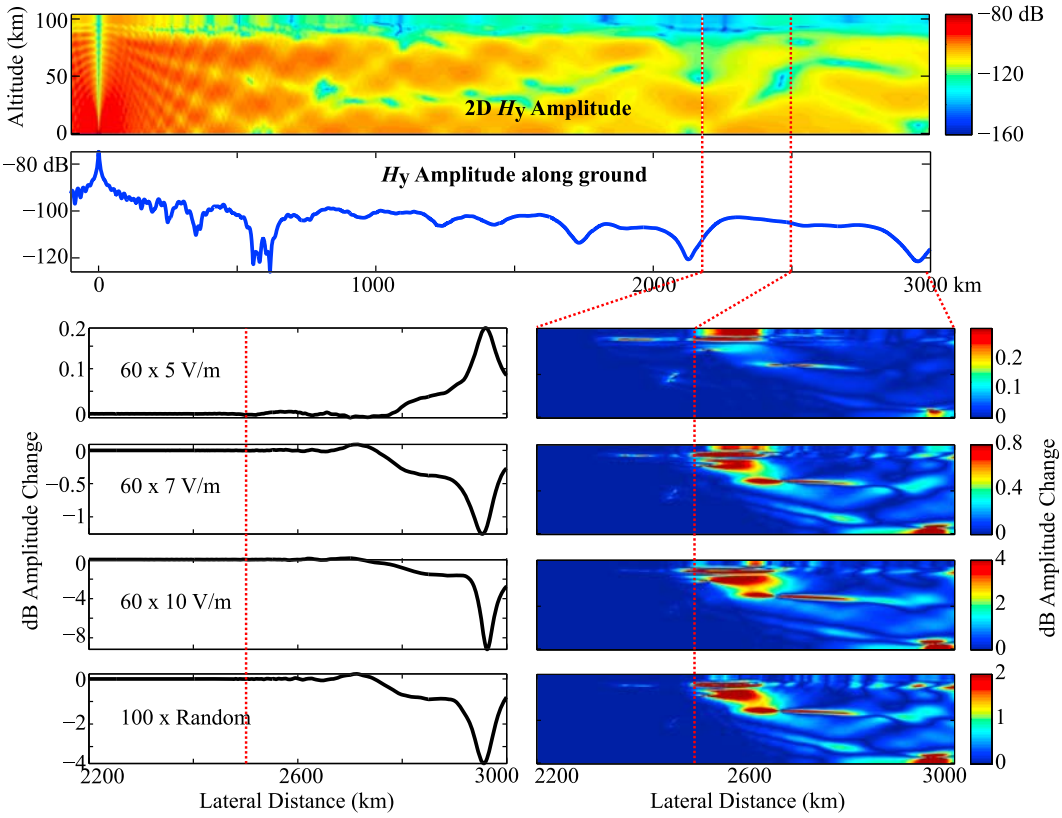


Figure 8. VLF transmitter propagation simulation with EMP multipulse inputs on a 3000 km path. The top two panels repeat the ambient 2-D and 1-D along-ground amplitudes. The bottom panels show the scattered 2-D and 1-D fields for the four cases of *Marshall et al.* [2010]. In this case the path is only 3000 km and the perturbation is 500 km from the receiver (denoted by the vertical dashed red line in the bottom panels).

[43] Note that the sferic bursts simulated in the work by *Marshall et al.* [2010] and applied here are independent of total time; that is, they do not assume an interpulse wait time, and are valid for any such time duration, as long as that time is long enough so that the pulses do not overlap and interfere. *Marshall et al.* [2007] presented sferic bursts with durations ranging from 20 ms to 3 s; as such, these simulated disturbances could also accumulate on any time scale in that range. Therefore, the results in the present work are applicable for early/fast or early/slow events; "fast" and "slow" are not clearly delineated. In the case of early/fast events, however, it is very likely that other mechanisms may be responsible for many, or even most, events.

5. Discussion and Conclusions

[44] In this work we have presented a frequency domain method for modeling subionospheric VLF perturbations, and shown that electron density disturbances in the lower ionosphere caused by sequences of in-cloud pulse discharges can produce perturbations that are in general measurable by VLF techniques. Thus, some early VLF events may be the signature of sferic burst–associated electron density changes in the lower ionosphere. This scenario is the most likely among current mechanisms for the production of early/slow events; the longer risetime of these events corresponds very well with the duration of sferic bursts, suggesting that the latter is responsible for the former. In addition, *Haldoupis et al.* [2006] regularly observed sferic bursts at the onset of early/slow events, suggesting their possible involvement in the slow build up of the amplitude change. Note, however, that our method is limited by its inability to simulate finite-width disturbances or off-path disturbances, which may affect the received amplitudes to some degree.

[45] This mechanism is also the most likely candidate for early VLF events which do not correlate with sprites, as observed by *Marshall et al.* [2006], or other events for which the charge moment change is not large enough to produce QE breakdown. However, it should be noted that other mechanisms for early VLF events (QE breakdown and quiescent heating, in particular) may also be responsible for some early VLF events, and in some cases multiple mechanisms will be working in concert. To ascertain the specific causes for any particular early VLF event will require detailed knowledge of the causative lightning (both CG and in-cloud components), as well as the ionospheric conditions along the entire VLF propagation path.

[46] In this paper we have also shown that the received amplitude, as well as its polarity, is strongly dependent on a number of parameters: in particular, the path length, ionospheric and ground parameters, and transmitter frequency all affect the received amplitude very nonlinearly, and can lead to small, even unmeasurable perturbations even for signifi-

cant ionospheric disturbances. We have found that the ambient ionospheric electron density, however, does not have a strong effect on received amplitudes. These results imply that the absence of a measured perturbation to the VLF signal does not imply a lack of disturbance in the ionosphere. Furthermore, recall the results of *Marshall et al.* [2010], wherein it was found that the electron density disturbance is very nonlinearly related to the parameters of the constitutive pulses in a sferic burst, including altitude, pulse duration (i.e., speed), orientation, latitude, and amplitude. These parameters are difficult, if not impossible, to measure completely in a particular sferic burst event. As such, the two processes modeled in the work by *Marshall et al.* [2010] and the present work, namely the electron density disturbance and the VLF amplitude perturbation, together show the importance of modeling in understanding and quantifying these processes. Qualitatively, our modeling work has shown that such in-cloud bursts, of which sferic bursts are the VLF signature, may account for a number of observed early/fast and early/slow VLF perturbations.

[47] **Acknowledgments.** This work was supported by Office of Naval Research grant N00014-03-1-0333 and National Science Foundation grant ATM-0551174.

[48] Zuyin Pu thanks Robert Moore and Agnes Mika for their assistance in evaluating this paper.

References

Armstrong, W. C. (1983), Recent advances from studies of the Trimpi effect, *Antarct. J. U. S.*, *18*, 281–283.

Barrington-Leigh, C. P., U. S. Inan, and M. Stanley (2001), Identification of sprite and elves with intensified video and broadband array photometry, *J. Geophys. Res.*, *106*(A2), 1741–1750.

Berger, K., R. B. Anderson, and H. Kroninger (1975), Parameters of lightning flashes, *Electra*, *80*, 223–237.

Budden, K. G. (1961), *The Wave-Guide Mode Theory of Wave Propagation*, Prentice-Hall, Englewood Cliffs, N. J.

Cheng, Z., and S. A. Cummer (2005), Broadband VLF measurements of lightning-induced ionospheric perturbations, *Geophys. Res. Lett.*, *32*, L08804, doi:10.1029/2004GL022187.

Cheng, Z., S. A. Cummer, H.-T. Su, and R.-R. Hsu (2007), Broadband very low frequency measurement of *D* region ionospheric perturbations caused by lightning electromagnetic pulses, *J. Geophys. Res.*, *112*, A06318, doi:10.1029/2006JA011840.

Chevalier, M. W., and U. S. Inan (2006), A technique for efficiently modeling long-path propagation for use in both FDFD and FDTD, *IEEE Antennas Wireless Propag. Lett.*, *5*, 525–528.

Chevalier, T. W., U. S. Inan, and T. F. Bell (2008), Terminal impedance and antenna current distribution of a VLF electric dipole in the inner magnetosphere, *IEEE Trans. Antennas Propag.*, *56*(8), 2454–2468.

Dowden, R. L., and C. D. D. Adams (1990), Location of lightning-induced electron precipitation from measurement of VLF phase and amplitude perturbations on spaced antennas and on two frequencies, *J. Geophys. Res.*, *95*(A4), 4135–4145.

Dowden, R. L., C. D. D. Adams, J. B. Brundell, and P. E. Dowden (1994), Rapid onset, rapid decay (RORD), phase and amplitude perturbations of VLF subionospheric transmissions, *J. Atmos. Terr. Phys.*, *56*, 1513–1527.

Dowden, R. L., J. B. Brundell, W. A. Lyons, and T. E. Nelson (1996), Detection and location of red sprites by VLF scattering of subionospheric transmissions, *Geophys. Res. Lett.*, *23*(14), 1737–1740.

Ferguson, J. A., and F. P. Snyder (1987), The segmented waveguide program for long wavelength propagation calculations, *Tech. Rep. 1071*, Nav. Ocean Syst. Cent., San Diego, Calif.

Haldoupis, C., T. Neubert, U. S. Inan, A. Mika, T. H. Allin, and R. A. Marshall (2004), Subionospheric early VLF signal perturbations observed in one-to-one association with sprites, *J. Geophys. Res.*, *109*, A10303, doi:10.1029/2004JA010651.

Haldoupis, C., R. J. Steiner, Á. Mika, S. Shalimov, R. A. Marshall, U. S. Inan, T. Bösinger, and T. Neubert (2006), "Early/slow" events: A new category of VLF perturbations observed in relation with sprites, *J. Geophys. Res.*, *111*, A11321, doi:10.1029/2006JA011960.

Inan, U. S., D. C. Shafer, W. P. Yip, and R. E. Orville (1988), Subionospheric VLF signatures of nighttime *D* region perturbations in the vicinity of lightning discharges, *J. Geophys. Res.*, *93*(A10), 11,455–11,472.

Inan, U. S., T. F. Bell, and J. V. Rodriguez (1991), Heating and ionization of the lower ionosphere by lightning, *Geophys. Res. Lett.*, *18*(4), 705–708.

Inan, U. S., V. P. Pasko, and T. F. Bell (1996a), Sustained heating of the ionosphere above thunderstorms as evidenced in "early/fast" VLF events, *Geophys. Res. Lett.*, *23*(10), 1067–1070.

Inan, U. S., S. C. Reising, G. J. Fishman, and J. M. Horack (1996b), On the association of terrestrial gamma-ray bursts with lightning and implications for sprites, *Geophys. Res. Lett.*, *23*(9), 1017–1020.

Inan, U. S., A. Slingeland, V. P. Pasko, and J. V. Rodriguez (1996c), VLF and LF signatures of mesospheric/lower ionospheric response to lightning discharges, *J. Geophys. Res.*, *101*(A3), 5219–5238.

Johnson, M. P., and U. S. Inan (2000), Sferic clusters associated with early/fast VLF events, *Geophys. Res. Lett.*, *27*(9), 1391–1394.

Johnson, M. P., U. S. Inan, S. J. Lev-Tov, and T. F. Bell (1999), Scattering pattern of lightning-induced ionospheric disturbances associated with early/fast VLF events, *Geophys. Res. Lett.*, *26*(15), 2363–2366.

Lev-Tov, S. J., U. S. Inan, and T. F. Bell (1995), Altitude profiles of localized *D* region density disturbances produced in lightning-induced electron precipitation events, *J. Geophys. Res.*, *100*(A11), 21,375–21,383.

Lev-Tov, S. J., U. S. Inan, A. J. Smith, and M. A. Clilverd (1996), Characteristics of localized ionospheric disturbances inferred from VLF measurements at two closely spaced receivers, *J. Geophys. Res.*, *101*(A7), 15,737–15,747.

Marshall, R. A., U. S. Inan, and W. A. Lyons (2006), On the association of early/fast very low frequency perturbations with sprites and rare examples of VLF backscatter, *J. Geophys. Res.*, *111*, D19108, doi:10.1029/2006JD007219.

Marshall, R. A., U. S. Inan, and W. A. Lyons (2007), Very low frequency sferic bursts, sprites, and their association with lightning activity, *J. Geophys. Res.*, *112*, D22105, doi:10.1029/2007JD008857.

Marshall, R. A., U. S. Inan, and T. W. Chevalier (2008), Early VLF perturbations caused by lightning EMP-driven dissociative attachment, *Geophys. Res. Lett.*, *35*, L21807, doi:10.1029/2008GL035358.

Marshall, R. A., U. S. Inan, and V. S. Glukhov (2010), Elves and associated electron density changes due to cloud-to-ground and in-cloud lightning discharges, *J. Geophys. Res.*, *115*, A00E17, doi:10.1029/2009JA014469.

Mende, S. B., H. U. Frey, R. R. Hsu, H. T. Su, A. B. Chen, L. C. Lee, D. D. Sentman, Y. Takahashi, and H. Fukunishi (2005), *D* region ionization by lightning-induced electromagnetic pulses, *J. Geophys. Res.*, *110*, A11312, doi:10.1029/2005JA011064.

Mika, A. (2007), Very low frequency EM wave studies of transient luminous events in the lower ionosphere, Ph.D. thesis, Univ. of Crete, Crete, Greece.

Mika, A., C. Haldoupis, T. Neubert, R. R. Su, H. T. Hsu, R. J. Steiner, and R. A. Marshall (2006), Early VLF perturbations observed in association with elves, *Ann. Geophys.*, *24*, 2179–2189.

Moore, R. C., C. P. Barrington-Leigh, U. S. Inan, and T. F. Bell (2003), Early/fast VLF events produced by electron density changes associated with sprite halos, *J. Geophys. Res.*, *108*(A10), 1363, doi:10.1029/2002JA009816.

Orville, R. E. (1991), Calibration of a magnetic direction finding network using measured triggered lightning return stroke peak currents, *J. Geophys. Res.*, *96*(D9), 17,135–17,142.

Pappert, R. A., and F. P. Snyder (1972), Some results of a mode-conversion program for VLF, *Radio Sci.*, *7*, 913–923.

Pasko, V. P., and U. S. Inan (1994), Recovery signatures of lightning-associated VLF perturbations as a measure of the lower ionosphere, *J. Geophys. Res.*, *99*(A9), 17,523–17,537.

Pasko, V. P., U. S. Inan, and T. F. Bell (1998), Ionospheric effects due to electrostatic thundercloud fields, *J. Atmos. Sol. Terr. Phys.*, *60*, 863–870.

Peter, W. B., and U. S. Inan (2007), A quantitative comparison of lightning-induced electron precipitation and VLF signal perturbations, *J. Geophys. Res.*, *112*, A12212, doi:10.1029/2006JA012165.

Poulsen, W. L., T. F. Bell, and U. S. Inan (1990), Three-dimensional modeling of subionospheric VLF propagation in the presence of localized *D* region perturbations associated with lightning, *J. Geophys. Res.*, *95*(A3), 2355–2366.

Poulsen, W. L., U. S. Inan, and T. F. Bell (1993), A multiple-mode three-dimensional model of VLF propagation in the Earth-ionosphere waveguide in the presence of localized *D* region disturbances, *J. Geophys. Res.*, *98*(A2), 1705–1717.

Ratcliffe, J. A. (1959), *The Magneto-Ionic Theory and Its Applications to the Ionosphere*, Cambridge Univ. Press, Cambridge, U. K.

Taflove, A., and S. C. Hagness (2005), *Computational Electrodynamics: The Finite-Difference Time-Domain Method*, 3rd ed., Artech House, Boston, Mass.

Taranenko, Y. N., U. S. Inan, and T. F. Bell (1993), Interaction with the lower ionosphere of electromagnetic pulses from lightning: Heating, attachment, and ionization, *Geophys. Res. Lett.*, *20*(15), 1539–1542.

Tolstoy, A. (1983), The influence of localized precipitation-induced *D* region ionization enhancements on subionospheric VLF propagation, Ph.D. thesis, Univ. of Md., College Park.

Tolstoy, A., T. J. Rosenberg, U. S. Inan, and D. L. Carpenter (1986), Model predictions of subionospheric VLF signal perturbations resulting from localized, electron precipitation-induced ionization enhancement regions, *J. Geophys. Res.*, *91*(A12), 13,473–13,482.

Walt, M. (1994), *Introduction to Geomagnetically Trapped Radiation*, Cambridge Univ. Press, Cambridge, U. K.

U. S. Inan, STAR Laboratory, Stanford University, 350 Serra Mall, Room 354, Stanford, CA 94305, USA.

R. A. Marshall, Center for Space Physics, Boston University, 725 Commonwealth Ave., Boston, MA 02215, USA. (robertm@bu.edu)